Faraday
Discussions

Water dynamics and sum-frequency generation spectra at electrode/aqueous electrolyte interfaces

Journal:	*Faraday Discussions*
Manuscript ID	FD-ART-05-2023-000103.R1
Article Type:	Paper
Date Submitted by the Author:	12-Jun-2023
Complete List of Authors:	Olivieri, Jean-Francois; Ecole Normale Superieure Hynes, James; Ecole Normale Superieure; University of Colorado Laage, Damien; Ecole Normale Supérieure

SCHOLARONE™
Manuscripts

Journal Name

Water dynamics and sum-frequency generation spectra at electrode/aqueous electrolyte interfaces

Jean-François Olivieri,[a] James T. Hynes,[ab] and Damien Laage[a*]

The dynamics of water at interfaces between an electrode and an electrolyte are essential for the transport of redox species and for the kinetics of charge transfer reactions next to the electrode. However, while the effects of electrode potential and ion concentration on the electric double layer structure have been extensively studied, a comparable understanding of dynamical aspects is missing. Interfacial water dynamics present challenges since they are expected to result from the complex combination of water-electrode and water-ion interactions. Here we perform molecular dynamics simulations of aqueous NaCl solutions at the interface with graphene electrodes and examine the impact of both ion concentration and electrode potential on interfacial water reorientational dynamics. We show that for all salt concentrations water dynamics exhibits a strongly asymmetric behavior: it slows down at increasingly positively charged electrodes but it accelerates at increasingly negatively charged electrodes. At negative potentials water dynamics is determined mostly by the electrode potential value, but in contrast at positive potentials it is governed both by ion-water and electrode-water interactions. We show how these strikingly different behaviors are determined by the interfacial hydrogen-bond network structure and by the ions' surface affinity. Finally, we indicate how the structural rearrangements impacting water dynamics can be probed via vibrational sum-frequency generation spectroscopy.

Introduction

Interfaces between an aqueous electrolyte and an electrode play a key role in a broad range of fundamental chemical processes including, e.g., energy conversion via photocatalytic water splitting, energy storage in batteries, and carbon dioxide reduction. Accordingly, a major effort, both experimental and theoretical, is being devoted to gaining a better comprehension of these interfaces[1,2]. However, despite important advances, key gaps remain in our molecular-level understanding of such interfaces' structure and dynamics.

Here we focus on two key questions. The first pertains to the structure of the electrical double layer formed at the electrode and how it changes with the applied electrode potential. Textbook descriptions of electrode/electrolyte interfaces traditionally rely on mean-field continuum pictures due to Hemholtz, Gouy, Chapman and Stern[3]. While these have been valuable guides for electrochemistry, it is well known that they miss important aspects; these include the discrete nature of water molecules and ions, ion correlations, specific molecular interactions and non-local effects[1]. Vibrational sum-frequency generation (SFG) spectroscopy offers an incisive experimental approach to selectively probe the interface and the orientational arrangement of water molecules[1,4,5]. However, interpreting these spectra can be ambiguous: the respective contributions from the first so-called Stern layer and the diffuse layer are difficult to disentangle[1,6–8].

The second question deals with the electrode's impact on the electrolyte dynamics. While most studies so far have focused on structural aspects, the dynamics of interfacial water molecules has been much less examined, despite its essential role for the transport of redox species to and away from these interfaces and for the kinetics of interfacial charge transfer reactions.

The structure of the electrical double layer at charged surfaces has been extensively studied with both SFG spectroscopy experiments and molecular simulations using charged silica surfaces (see, e.g. refs.[5,9–14]). These studies have investigated, e.g., how the double layer structure varies with surface charge and the nature of the salt. However, a complexity arises here, since changing the silica surface charge is achieved by shifting the pH, which also implies changing the interface's chemical properties.

An alternate, and particularly attractive, prototypical electrified/aqueous solution interface is thus provided by graphene electrodes. In addition to its promising technological applications, graphene combines several important advantages: i) due to its semi-metallic nature, an external electric potential can be applied to control its surface charges; ii) buried water-electrode interfaces

[a] PASTEUR, Department of Chemistry, École normale supérieure, PSL University, Sorbonne Université, CNRS, 75005 Paris, France. Email: damien.laage@ens.psl.eu
[b] Department of Chemistry, University of Colorado, Boulder, Colorado 80309, United States

are challenging for SFG experiments, while the IR-transparent graphene sheet allows more incoming IR beam transmission than does a metal, iii) it provides a well-defined, atomically flat, interface. The feasibility of this graphene-based approach was recently demonstrated in pioneering SFG experiments on interfaces between electrified graphene and neat water[15–20]. In addition, in molecular simulations by some of us[21,22], characterization of the dynamics of water molecules in contact with an electrified graphene interface showed that interfacial water dynamics is markedly different at positive and negative electrodes. While water reorientation dynamics is increasingly slowed down as the magnitude of an applied positive electrode potential increases, it changes in a non-monotonic fashion with the potential at negatively charged electrodes.

However, these just-described experimental and simulation results were obtained in the neat water situation; the key question of the impact of a salt on the interfacial properties at different electrode potentials thus remains unaddressed.

The present first effort to deal with this absence focuses on the paradigm interface between electrified graphene and NaCl aqueous solutions. We use molecular dynamics simulations to determine how the structure and dynamics of the interfacial water layer is affected by the electrode potential and by the salt. Further, we indicate how the combined impacts of the electrode and the ions on the interfacial structure are reflected in experimentally-accessible SFG spectra.

In the remainder of this contribution, we first describe our simulation methodology and determine the respective salt and electrode impacts on the interfacial water reorientation dynamics. We then characterize the structure of the electrical double layer and the orientation of the interfacial water molecules as salt is added and as the electrode potential is increased. Next, we calculate the SFG spectra and determine the interfacial and diffuse layer contributions. Finally, we offer some concluding remarks.

Methodology

Our simulation methodology extends the procedure described in our prior studies[21,22] of neat water/electrified graphene interfaces to include Na^+Cl^- ions at concentrations ranging from 0.1 to 5 mol/L. We performed classical molecular dynamics simulations of a slab of water molecules confined between two parallel single graphene plates separated by a 60 Å distance. The rigid graphene sheets are constructed from an ideal hexagonal lattice with a 1.42 Å distance between neighboring carbon atoms and each 240-atom plate is periodically replicated in the two directions parallel to the graphene plane. The resulting simulation box dimensions are 24.58×25.54×60.00 Å^3. At each salt concentration, the number of water molecules is adjusted by an insertion/deletion procedure to match the experimental aqueous solution density[23,24]. The numbers of water molecules and of Na^+Cl^- ion pairs are respectively 1152/0 in neat water, 1152/2 at 0.1 mol/L, 1144/10 at 0.5 mol/L, 1133/21 at 1 mol/L, 1110/41 at 2 mol/L, 1083/62 at 3 mol/L, 1057/83 at 4 mol/L and 1033/104 at 5 mol/L. Water is described by the SPC/E potential[25] which has been shown[26] to provide an excellent description of water dynamics at ambient temperature. Ions are modeled by a

scaled-charge ECCR force field which was shown[27] to provide a good implicit description of polarizability effects, and especially of their impact on water dynamics. Graphene carbon Lennard-Jones parameters are taken from ref.[28] where they were optimized to reproduce DFT-based molecular dynamics simulation results. The carbon-ion dispersive Lennard-Jones terms are scaled by the same 0.7 factor as suggested in ref.[28] for the carbon-water oxygen interaction. Long-range electrostatic interactions are described via a two-dimensional Ewald summation method with the Yeh-Berkowitz slab correction[29]. Opposite electrostatic potentials are applied to the two graphene plates. In order to maintain the electrostatic potential at each electrode atom fixed, the graphene carbon atom charges are allowed to fluctuate. We employ the constant potential[30,31] method which has already been successfully used for a broad range of electrode/electrolyte interfaces. Graphene carbon charges are described by Gaussian distributions whose amplitudes are determined at every step, using the constant potential implementation of ref.[32]. The Gaussian inverse width is fixed to be 2.55 Å^{-1}, as suggested in ref.[33] for carbon atoms.

Molecular dynamics simulations were run with LAMMPS[34] for a series of electrode potentials ranging from 0 to ±2.5 V and for a series of salt concentrations from 0 to 5 mol/L. While similar electrode potentials have been used in experiments on neat water/electrified graphene interfaces[15], large voltages may cause electrode/electrolyte electron transfers in the presence of ions and they should only be considered to highlight the trends in our simulations. After an initial 1 ns-long equilibration, trajectories were propagated for 1 ns in the canonical ensemble at 298.15 K using a Nose-Hoover thermostat. Configurations were collected every 50 ps along this thermostatted trajectory. Our analyses are based on the independent microcanonical trajectories that were then propagated for 500 ps from these configurations, using a 10-fs output interval. All error bars reported in the following are 95% confidence intervals.

Phase-resolved vibrational SFG spectra were calculated using the empirical map developed in ref.[35] to connect the water OH bond dipole and polarizability tensor to the instantaneous electric field experienced by the water H atom along the OH direction. Our calculated spectra correspond to these that would be measured using a dilute HOD in a liquid D_2O solution, in order to decouple the local OH mode from other OD stretch modes in the liquid. The switching function suggested in ref.[36] and dependent on the distance between the oxygen atom and the middle of the water slab is applied to determine the SFG spectra at each electrode separately.

Interfacial water dynamics

Water reorientation dynamics

We first characterize the dynamics of water molecules at the electrode interface and how it is impacted by the salt and the electrode potential. We focus on water OH group reorientation dynamics and calculate the reorientation time-correlation function relevant for ultrafast infrared anisotropy and NMR measurements

$$C_2^{OH}(t) = \langle P_2 \left[\mathbf{u}_{OH}(0) \cdot \mathbf{u}_{OH}(t) \right] \rangle \quad (1)$$

where $\mathbf{u}_{OH}(t)$ is the unit vector along the water OH group direction, P_2 is the second-order Legendre polynomial and the $\langle...\rangle$ ensemble average is performed over all water OH groups within the first layer at t=0 (defined to include all water molecules whose oxygen atom is within 5 Å from the graphene plane[22]). We then determine the reorientation time τ_2^{OH} as the time integral of $C_2^{OH}(t)$. In prior simulation studies, we had already separately considered the impact of ions on water dynamics in the bulk (see, e.g., refs.[27,37,38]) and the impact of an electrode on neat water dynamics (see, e.g., refs.[21,22]). We now aim at determining how water dynamics is affected by the simultaneous combination of ions and of a charged electrode interface.

Impact of electrode potential

We consider how ions affect the way interfacial water dynamics changes with the electrode potential. Figure 1 contrasts the interfacial water reorientation times without ions and with 1 mol/L NaCl for a series of electrode potentials. The most striking result visible in Fig. 1 is that although this salt does not substantially affect interfacial water dynamics at negatively charged electrodes, it does have a large impact at positively charged electrodes.

Here it is useful to recall the neat water dynamical behavior that had been revealed in our recent studies[21,22]. In neat water, positive electrode potentials induce a large slowdown in water dynamics, as shown in Fig. 1. In contrast, increasingly negative potentials cause an acceleration of water dynamics, followed by a retardation for very negative potentials. The electrode's impact on water reorientation dynamics was determined to be short-ranged[21] and Fig. 1 shows that τ_2^{OH} in the middle of the water slab remains bulk-like and is almost insensitive to the electrode potential.
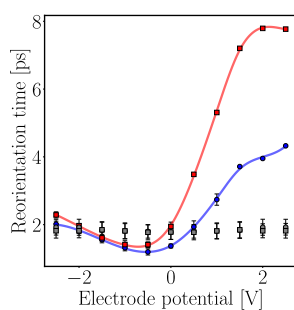

Fig. 1 Water reorientation time τ_2^{OH} for water OH groups initially in the first interfacial layer without salt (blue circles) and in the presence of 5 mol/L NaCl (red squares) for a series of electrode potentials. Grey symbols show the reorientation times of water OH groups in the middle of the slab, without salt (circles) and with 5 mol/L NaCl (squares).

In the presence of 1 mol/L NaCl, we first discuss the 0 V situation. Surprisingly, the introduction of salt has no significant effect on water dynamics in the middle of the slab. In contrast, in bulk solutions NaCl is known to cause a moderate slowdown of water dynamics[27,38]. For example, simulations using the same water and ion force field had shown[27] that in bulk 5 mol/L NaCl aqueous solution, τ_2^{OH} is slowed by $\simeq 1.2$ with respect to the neat water situation. In contrast, at the interface the salt increases the water

reorientation time by a $\simeq 1.4$ factor with respect to the neat water situation. We now turn to the impact of electrode potentials. For increasingly negative electrode potentials, the presence of salt does not change the behavior of interfacial water dynamics. We observe the same acceleration for moderately negative potentials and slowdown for very negative potentials as in the neat water case, even though the τ_2^{OH} values are slightly modified and the acceleration relative to the 0 V case is somewhat enhanced by the salt. In contrast, for increasingly positive electrode potentials, the presence of salt substantially enhances the slowdown of interfacial water reorientation dynamics. For the largest electrode potentials considered here, τ_2^{OH} is almost twice slower in the presence of salt than in its absence.

Impact of salt concentration

Next, we examine the impact of increasing salt concentration on interfacial dynamics at fixed electrode potentials, here chosen to be $\pm$ 0 V and $\pm$ 2.5 V. At the negative electrode, increasing the salt concentration causes a very moderate slowdown of interfacial water dynamics, and this retardation almost vanishes when the electrode potential absolute value increases (Fig. 2a). In contrast, at the positive electrode, adding more ions induces a pronounced slowdown, which markedly increases with increasing electrode potential (Fig. 2b).
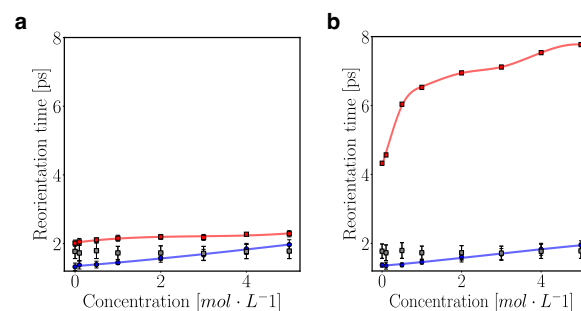

Fig. 2 Water reorientation time τ_2^{OH} for water OH groups initially in the first interfacial layer for increasing NaCl concentration at 0 V (blue) and at ± 2.5 V (red) a) at the negatively charged electrode and b) at the positively charged electrode. Grey symbols show the values in the middle of the slab, without salt (circles) and with 5 mol/L NaCl (squares).

Structure of interfacial layer

Our prior studies on a neat water slab between graphene electrodes had revealed the importance of interfacial water orientation and hydrogen-bond (H-bond) exchanges in determining water reorientation dynamics[21,22]. In order to provide a molecular interpretation to the above observations, we now examine the orientational arrangement of interfacial water molecules and the structure of the electric double layer.

Orientation of interfacial water molecules

To characterize the orientational arrangement of water molecules at the graphene electrode, we calculate the probability distribution of the angle θ between each water OH group and the vector normal to the interface oriented towards the nearest graphene

plate and of the distance Δz between the water H atom and the nearest graphene electrode (Fig. 3a). The reference situation of neat water next to the 0 V electrode reveals three distinct peaks in the water orientational distribution within the first layer (Fig. 3b). The first one corresponds to a small fraction of OH groups pointing towards the electrode ($\theta < 40°$, $\Delta z \simeq 2\text{Å}$). When the electrode is held at 0 V, carbon atoms are approximately apolar and these water OH groups are analogous to dangling OH groups at the air/water interface. The second peak arises from the largest fraction of interfacial OH groups which are tangent to the electrode surface ($\theta \simeq 90°$, $\Delta z \simeq 3.5\text{Å}$) and which are engaged in a H-bond with another interfacial water molecule. The third population corresponds to OH groups pointing away from the electrode and towards the liquid ($\theta > 140°$, $\Delta z \simeq 5\text{Å}$), donating a H-bond to a second-layer water molecule.

In the neat water case, our prior studies [21,22] have shown that the reorientation of interfacial water molecules due to surface charges is more complex than a simple dipole flip [13,15,39]. At the positive electrode the orientational arrangement of interfacial water molecules changes only marginally with the electrode potential (Fig. 3e). In contrast, at the negative electrode a substantial rearrangement occurs (Fig. 3c), which is responsible for the observed acceleration in interfacial reorientation dynamics. Due to the increasingly favorable interaction between water OH group and the graphene electrode when the potential is more negative and the graphene carbon atoms are more negatively charged, the fraction of interfacial water OH groups pointing towards the electrode grows. This is manifest in the change in probability distribution with respect to the 0 V neat water situation shown in Fig. 3c. This structural rearrangement impacts the water dynamics because τ_2^{OH} reorientation times depend on the OH group initial orientation. For tangent OH groups, the reorientation dynamics is moderately retarded with respect to that in the bulk due to the reduced number of potential H-bond acceptors to which these OH groups can jump and form a new H-bond. In contrast, because OH groups pointing towards the moderately negative electrode are engaged in an interaction which is weaker than that of an H-bond with another water molecule, their reorientation dynamics is facilitated with respect to that in the bulk, and therefore faster (for very negative electrode potentials, the interaction becomes stronger than a water-water H-bond and the reorientation dynamics is slower than in the bulk). The growing fraction of OH groups pointing towards the interface and whose reorientation is fast thus causes the observed acceleration in average interfacial dynamics at moderately negative electrodes.

We therefore examine how the interfacial orientational arrangement is impacted by the addition of salt. Figures 3d and 3f present the changes in probability distribution between neat water at the 0 V interface and 5 mol/L NaCl at the -2.5 V and +2.5 V electrodes respectively. They show that at both electrodes the interfacial structural rearrangement in the presence of salt is qualitatively similar to that in the absence of salt. The negative electrode potential (Fig. 3d) causes an enrichment in the population pointing towards the electrode and a depletion of the H-bonded populations either tangent to the interface or pointing towards the slab, and these population transfers are slightly en-
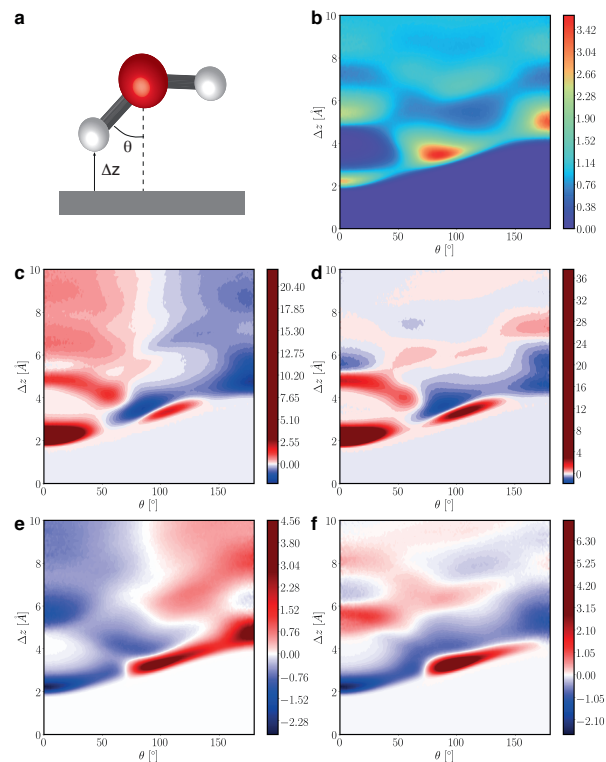

Fig. 3 a) Coordinates used to describe the orientation of interfacial water OH groups: angle θ between a water OH and the surface normal vector and distance Δz between the water H atom and the nearest graphene plane. Normalized probability distributions b) for a neat water slab at 0 V, c) change in probability for neat water when charging the electrode from 0 V to -2.5 V, d) change in probability when going from neat water at 0 V to 5 mol/L NaCl at the -2.5 V electrode, e) change in probability for neat water when charging the electrode from 0 V to +2.5 V, f) change in probability when going from neat water at 0 V to 5 mol/L NaCl at the +2.5 V electrode.

hanced by the addition of salt. The positive electrode potential induces a depletion in the population pointing towards the interface. The impact of added salt on interfacial water dynamics at the positive electrode thus does not appear to be caused by a substantial change in the equilibrium between water OH groups pointing towards the interface and towards an H-bond acceptor. However, we note that the most important effect caused by the ions is the strong depletion in water OH groups pointing away from the positively charged electrode (Fig. 3f), and we will investigate its cause and implications in the following.

Ion density profiles

To further characterize the structure of the aqueous solution at the electrode interface, we calculate the density profiles of the Na^+ and Cl^- ions along the axis between the two graphene plates, shown in Fig. 4 for NaCl aqueous solutions of increasing concentrations between electrodes held at ±2.5 V. It reveals a striking difference between the Cl^- anions and Na^+ cations: while the Cl^- anions strongly adsorb at the positively charged electrode, the Na^+ cations display a much weaker affinity for the negative electrode. In addition, these results obtained from molecular dynamics simulations differ in several important ways from the pre-

dictions of mean-field theories. First, the electrical double layer terminology is misleading, since even next to the Cl$^-$ anions that strongly adsorb at the electrode no compensating layer of Na$^+$ cations forms in the second layer. The second aspect relates to the proposed Stern layer: we see that this description is much more adequate for Cl$^-$ anions than for Na$^+$ cations. In addition, even for Cl$^-$, this layer should not be described as compact: for the solution of 5 mol/L average concentration, the local Cl$^-$ number density at the positive electrode implies that the effective concentration is approximately 8 mol/L, with anion-anion nearest neighbor distances of $\simeq$14 Å, much larger than the contact distance. Finally, the diffuse layer is shown to strongly differ from the exponential distribution expected from mean-field models, which again stresses the importance of accounting for specific molecular interactions.
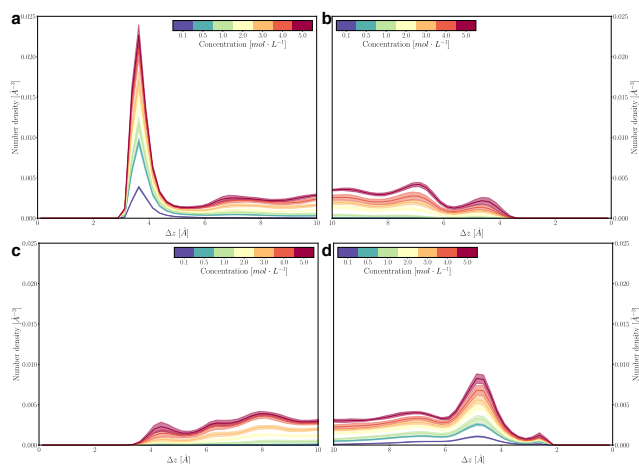

Fig. 4 Ion density profiles for NaCl aqueous solutions along the distance to the nearest graphene plate, a) for Cl$^-$ at the +2.5 V electrode, b) for Cl$^-$ at the -2.5 V electrode, c) for Na$^+$ at the +2.5 V electrode and d) for Na$^+$ at the -2.5 V electrode.

Interpretation of ions' impact on interfacial water dynamics

The dramatically different behaviors of Na$^+$ and Cl$^-$ ions thus provide the molecular explanation for the contrasted impacts of ions on interfacial water dynamics (Fig. 1). Adding NaCl does not markedly change water reorientation dynamics at negatively charged electrodes because of the low propensity of ions to adsorb at this interface: water dynamics is thus governed by the water-electrode interactions and accelerated at moderately negative electrode potentials. In contrast, at the positively charged interface, the effective local concentration in Cl$^-$ anions is much larger than in the bulk solution, and water dynamics is controlled both by water-electrode and by water-ion interactions. We had shown in prior works[40,41] that water reorientation dynamics proceeds via two pathways: large-angular jumps caused by H-bond exchanges and diffusive tumbling of the local frame between successive H-bond exchanges. In a recent simulation study[27], we showed that the slowdown caused by NaCl mostly arises from the retardation of the frame component, due to the salt-induced viscosity increase. The local increase in anion concentration at the positive electrode (Fig. 4) thus causes the slowdown of wa-

ter reorientation seen in Fig. 1. In addition, the presence of Cl$^-$ anions in the interfacial layer explains the partial orientational rearrangement of interfacial water molecules shown in Fig. 3f: the depletion in water OH groups pointing towards the slab upon adding salt is due to the reorientation of interfacial molecules in order to donate H-bonds to the Cl$^-$ ions. Finally, the preferential adsorption of ions at the interface leads to a decrease in the local salt concentration in the middle of the slab, and explains the smaller effect on water reorientation dynamics in the middle of the slab than in bulk solutions with the same average concentration.

Vibrational sum-frequency generation spectra

We now examine whether the structural rearrangements of water at electrodes in the presence of salt shown here via simulations can be probed experimentally via SFG spectroscopy.

We note that the first SFG spectra of water at electrified graphene interfaces[15] employed a support layer which was recently suggested[20] to significantly affect the measured signal. Alternative setups with a free-standing graphene sheet[17,18] thus offer a promising route to exclusively probe the effect of the electrified graphene on the interfacial water molecules, including in the presence of ions[18]. Our simulated system resembles these free-standing setups, with the notable difference of the obviously shorter distance between the oppositely charged electrodes.

Spectra

We calculate the resonant susceptibility accessible in SFG measurements with heterodyne detection and in the ssp polarization scheme

$$\chi^{(2)}_{xxz,yyz}(\omega) = \frac{i\omega}{k_B T} \int_0^\infty dt \ e^{i\omega t} \langle \alpha_{xx,yy}(t)\mu_z(0) \rangle \qquad (2)$$

where α is the water polarizability tensor and μ is the dipole moment, both determined at every step of the simulation from the local electric field using the empirical map developed in ref.[35].

When salt is added to the solution, the most dramatic impact on SFG spectra at both electrodes is the spectacular disappearance of the H-bonded band centered on 3400 cm^{-1} (Fig. 5). This band is known to arise from the static electric field created by the electrodes throughout the entire slab, which breaks the local symmetry and induces an SFG response. The progressive screening of this static field by the ions at the interface is thus expected to cause the strong decrease of this band's amplitude. However, closer analysis of the spectra reveals that the salt effect is more complex than a simple screening, since a change in the sign of the SFG susceptibility is discernable for example at the positive electrode for the larger salt concentrations. We therefore successively examine the SFG signals caused by the static field in the diffuse layer and by the interfacial layer.

Signal caused by static field

The long-range, so called $\chi^{(3)}$, signal caused by the static field created by charged interfaces has already been amply discussed[5,6,8,16,42–45] and we have shown its importance for neat
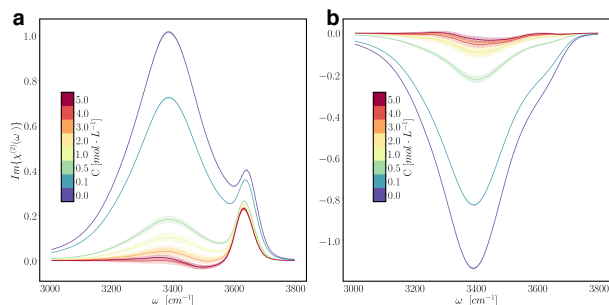
Fig. 5 Calculated phase-resolved SFG spectra of water a) at the -0.5 V electrode and b) at the +0.5 V electrode, both for increasing NaCl concentrations.

Fig. 6 a) Mean electrical potential profile across the cell between electrodes held at ± 0.5 V for solutions of increasing NaCl concentration; b) electric field in the middle of the cell for increasing external field imposed by the electrodes in neat water (blue) and with 1 mol/L (red) and 5 mol/L (green) NaCl (dashes show the field expected from a homogeneous slab description).

water at electrified graphene interfaces in prior work[22]. In electrolytes, this signal arises from the diffuse layer and must be subtracted from the collected total SFG signal in order to gain specific information about the interfacial layer, which is key, e.g., for electrochemical reactions. This diffuse layer signal is proportional to the static electric field in the diffuse layer, and determining this field is critical to subtract the diffuse layer's signal. We calculated the electrostatic potential in the cell by solving the Poisson equation following our prior work[22] and Fig. 6a shows that beyond a few molecular layers from the electrode, the slope of the potential, i.e., the field, is constant. However, Fig. 6a further reveals the strong salt-dependent screening of the electrode field by the first few molecular layers. As shown in Fig. 6b, the field in the middle of the cell is much smaller than the external field imposed by the electrodes. A supplementary difficulty is added by the salt's impact which changes with the external field. These results thus show that the static field cannot be obtained from mean-field descriptions and that subtracting the diffuse layer $\chi^{(3)}$ signal from the experimental spectrum is far from straightforward.

Signal due to interfacial layers

We finally turn to the SFG signal produced by the first molecular layers at the electrode interface. The results in Fig. 7 show that SFG spectra reveal important structural rearrangements caused by the ions, and that these effects are not restricted to the first layer but extend at least to the third molecular layer. We now show that these changes in the SFG signal can be interpreted via the structural analysis of Figs. 3-4.

At the negatively charged electrode, ions are shown to have a limited impact on the SFG spectra, in line with the small orientational rearrangement of interfacial water molecules in Fig. 3d. The largest change in the SFG signal comes from the second and third layers, due to the reorientation of water molecules caused by the presence of Na$^+$ cations in the second layer (Fig. 4).

Changes in the SFG contributions at the positive electrode are more dramatic. Ion-induced spectral changes in the first layer are explained by the orientational rearrangement shown in Fig. 3f: water OH groups that used to point away from the interface (leading to a negative $\chi^{(2)}$) in the absence of salt reorient to donate a H-bond to Cl$^-$ ions present in the first layer, leading to a red-shifted positive contribution that grows with ion concentration
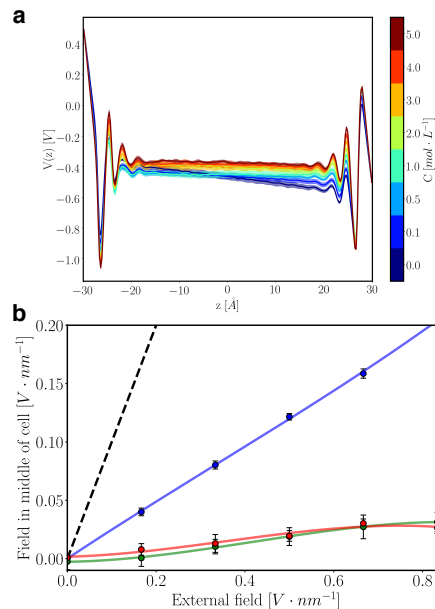
and a decrease of the negative-going band. In the second and third layers, the $\chi^{(2)}$ signal is observed to change sign at some frequencies. This is again ascribed to the reorientation of water OH groups that increasingly point towards the Cl$^-$ ions within the first layer when the salt concentration increases (see Fig. 3f).

Concluding remarks

Our study reveals that the impact of an electrified interface on the interfacial structure and dynamics of an aqueous electrolyte is strongly asymmetric with respect to the electrode potential. This arises from the molecular structure of water; the molecules' orientations are governed by H-bond formation more than by dipole-field interactions, and by the different surface propensities of anions and cations. For NaCl aqueous solutions, our results show that ions have a much larger structural and dynamical impact at the positive electrode due to the Cl$^-$ strong surface affinity. We show that the structural rearrangements of the water H-bond network and of the electrical double layer that cause the observed slowdown in water dynamics have an impact on the SFG spectra. However, determination of the SFG signal arising from the interfacial layers is not straightforward. It requires subtraction of the contribution from the diffuse layer: this scales with the static field in the middle of the cell, and due to interfacial screening this field is strongly reduced from the external field. Further studies will examine in detail how the nature of the salt affects the properties of electrode/electrolyte interfaces.

Conflicts of interest

There are no conflicts to declare.

Acknowledgements

Notes and references

1 G. Gonella, E. H. Backus, Y. Nagata, D. J. Bonthuis, P. Loche, A. Schlaich, R. R. Netz, A. Kühnle, I. T. McCrum, M. T. Koper, M. Wolf, B. Winter, G. Meijer, R. K. Campen and M. Bonn, *Nat Rev Chem*, 2021, **5**, 466–485.

2 J. Wu, *Chem Rev*, 2022, **122**, 10821–10859.

3 A. J. Bard and L. R. Faulkner, *Electrochemical Methods: Fundamentals and Applications*, Wiley, NY, 2001.

4 Y. R. Shen, *Annu Rev Phys Chem*, 2013, **64**, 129–150.

5 S. Nihonyanagi, S. Yamaguchi and T. Tahara, *Chem Rev*, 2017, **117**, 10665–10693.

6 Y. Wen, S. Zha, X. Liu, S. Yang, P. Guo, G. Shi, H. Fang, Y. Shen and C. Tian, *Phys Rev Lett*, 2016, **116**, 016101.

7 A. M. Darlington, T. A. Jarisz, E. L. DeWalt-Kerian, S. Roy, S. Kim, M. S. Azam, D. K. Hore and J. M. Gibbs, *J Phys Chem C*, 2017, **121**, 20229–20241.
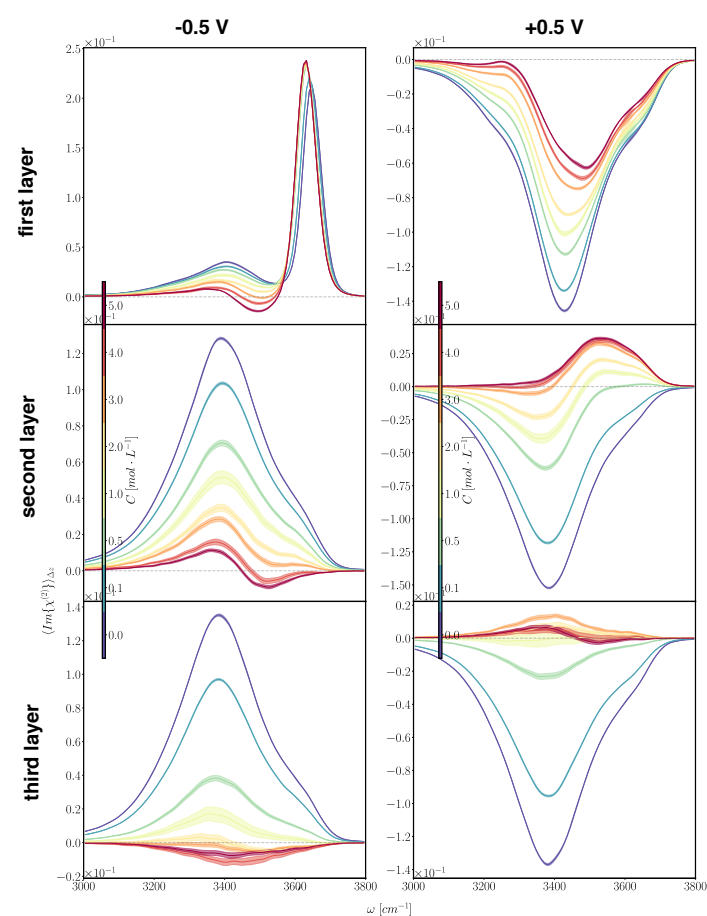
8 P. Ohno, H. Wang and F. Geiger, *Nat Commun*, 2017, **8**, 1032.

9 S. Urashima, A. Myalitsin, S. Nihonyanagi and T. Tahara, *J Phys Chem Lett*, 2018, **9**, 4109–4114.

10 J. Cyran, M. Donovan, D. Vollmer, F. Siro Brigiano, S. Pezzotti, D. Galimberti, M. Gaigeot, M. Bonn and E. Backus, *Proc Natl Acad Sci U S A*, 2019, **116**, 1520–1525.

11 J. Hunger, J. Schaefer, P. Ober, T. Seki, Y. Wang, L. Prädel, Y. Nagata, M. Bonn, D. Bonthuis and E. Backus, *J Am Chem Soc*, 2022, **144**, 19726–19738.

12 S. Dewan, V. Carnevale, A. Bankura, A. Eftekhari-Bafrooei, G. Fiorin, M. Klein and E. Borguet, *Langmuir*, 2014, **30**, 8056–8065.

13 B. Rehl, E. Ma, S. Parshotam, E. DeWalt-Kerian, T. Liu, F. Geiger and J. Gibbs, *J Am Chem Soc*, 2022, **144**, 16338–16349.

14 S. Chen and S. Singer, *J Phys Chem B*, 2019, **123**, 6364–6384.

15 A. Montenegro, C. Dutta, M. Mammetkuliev, H. Shi, B. Hou, D. Bhattacharyya, B. Zhao, S. Cronin and A. Benderskii, *Nature*, 2021, **594**, 62–65.

16 L. Dreier, Z. Liu, A. Narita, M. van Zadel, K. Müllen, K. Tielrooij, E. Backus and M. Bonn, *J Phys Chem C*, 2019, **123**, 24031–24038.

17 Y. Xu, Y.-B. Ma, F. Gu, S.-S. Yang and C.-S. Tian, *arXiv preprint arXiv:2207.08149*, 2022.

18 S. Yang, X. Zhao, Y. Lu, E. Barnard, P. Yang, A. Baskin, J. Lawson, D. Prendergast and M. Salmeron, *J Am Chem Soc*, 2022, **144**, 13327–13333.

19 M. Tsai, Y. Lu, C. Lin, C. Lin, C. Wang, C. Chu, W. Woon and C. Lin, *ACS Appl Mater Interfaces*, 2023, **15**, 17019–17028.

20 Y. Wang, T. Seki, X. Yu, C. Yu, K. Chiang, K. Domke, J. Hunger, Y. Chen, Y. Nagata and M. Bonn, *Nature*, 2023, **615**, E1–E2.

21 Y. Zhang, G. Stirnemann, J. T. Hynes and D. Laage, *Phys Chem Chem Phys*, 2020, **22**, 10581 – 10591.

22 Y. Zhang, H. B. de Aguiar, J. T. Hynes and D. Laage, *J Phys Chem Lett*, 2020, **11**, 624–631.

23 M. Laliberté and W. E. Cooper, *J Chem Eng Data*, 2004, **49**, 1141–1151.

24 S. Reiser, M. Horsch and H. Hasse, *J Chem Eng Data*, 2014, **59**, 3434–3448.

25 H. J. C. Berendsen, J. R. Grigera and T. P. Straatsma, *J Phys Chem*, 1987, **91**, 6269–6271.

26 J. Schmidt, S. Roberts, J. Loparo, A. Tokmakoff, M. Fayer and J. Skinner, *Chem Phys*, 2007, **341**, 143–157.

27 D. Laage and G. Stirnemann, *J Phys Chem B*, 2019, **123**, 3312–3324.

28 M. Rana and A. Chandra, *J Chem Phys*, 2013, **138**, 204702.

29 I.-C. Yeh and M. L. Berkowitz, *J Chem Phys*, 1999, **111**, 3155–3162.

30 J. I. Siepmann and M. Sprik, *J Chem Phys*, 1995, **102**, 511–524.

31 S. Reed, O. Lanning and P. Madden, *J Chem Phys*, 2007, **126**, 084704.

32 Z. Wang, Y. Yang, D. Olmsted, M. Asta and B. Laird, *J Chem Phys*, 2014, **141**, 184102.

Fig. 7 Imaginary part of the calculated phase-resolved SFG spectra of the first ($0 < \Delta z_O \leq 5$ Å), second ($5 < \Delta z_O \leq 8.7$ Å) and third ($8.7 < \Delta z_O \leq 11.9$ Å) molecular layers of water (where Δz_O is the distance from the water oxygen atom to the graphene plane) at the - 0.5 V electrode (left) and at the +0.5 V electrode (right) for increasing NaCl concentrations.

33 T. R. Gingrich and M. Wilson, *Chem Phys Lett*, 2010, **500**, 178–183.

34 S. Plimpton, *J Comp Phys*, 1995, **117**, 1–19.

35 B. Auer and J. Skinner, *J Chem Phys*, 2008, **129**, 214705.

36 Y. Ni and J. Skinner, *J Chem Phys*, 2016, **145**, 031103.

37 D. Laage and J. T. Hynes, *Proc Natl Acad Sci USA*, 2007, **104**, 11167–11172.

38 G. Stirnemann, E. Wernersson, P. Jungwirth and D. Laage, *J Am Chem Soc*, 2013, **135**, 11824–11831.

39 S. Nihonyanagi, S. Yamaguchi and T. Tahara, *J Chem Phys*, 2009, **130**, 204704.

40 D. Laage and J. T. Hynes, *Science*, 2006, **311**, 832–835.

41 D. Laage, G. Stirnemann, F. Sterpone, R. Rey and J. T. Hynes, *Annu Rev Phys Chem*, 2011, **62**, 395–416.

42 S. Ong, X. Zhao and K. B. Eisenthal, *Chem Phys Lett*, 1992, **191**, 327–335.

43 G. Gonella, C. Lütgebaucks, A. G. F. de Beer and S. Roke, *J Phys Chem C*, 2016, **120**, 9165–9173.

44 T. Joutsuka, T. Hirano, M. Sprik and A. Morita, *Phys Chem Chem Phys*, 2018, **20**, 3040–3053.

45 D. K. Hore and E. Tyrode, *J Phys Chem C*, 2019, **123**, 16911–16920.